Three-phase LCL-filter for Grid-connected Inverter Using Cooperative Bacteria Foraging Optimization

EHAB H.E. BAYOUMI
Department of Electrical and Electronics Engineering Technology
Abu Dhabi Men's College (ADMC), Higher Colleges of Technology
P.O. Box 25035, Abu Dhabi,
UNITED ARAB EMIRATES
ehab.bayoumi@gmail.com

Abstract: - This paper establishes an LCL-filters design and control for three-phase grid inverter. The crucial object is to conquer optimum damping with a required system control bandwidth for the LCL-filter. This control technique is achieved by using Bacteria Foraging Optimization. Mathematical analysis has been introduced to investigate the steady-state and dynamic performances of the overall system. The proposed control method is using one set of current sensors for feedback control only. The proposed system is simulated and results are demonstrated that bacterial foraging optimization is a skilful clarification for implementing the best parameters of LCL-filters and PI current controller. Results support the proposed technique and highlight its practicability.

Key-Words: - LCL-filter; grid-connected inverter; bacteria foraging optimization

1 Introduction

There is an ongoing increase in the number of embedded power sources connected to the power grid. The electrical output of many resources is incompatible with the fixed frequency electricity supply network; as a result power electronic interfacing is required. Power quality and transient performance of such distributed generation devices is dependent on inverter technology and control algorithms [1].

The voltage source grid-connected inverter (VSI) is one of the most important parts. A filter is required as an interface between the inverter and the power grid. Nowadays, *LCL*-filter is considered to be a preferred choice for its cost-effective attenuation of the switching frequency harmonics in the injected grid currents compared with *L*-filter. However, due to the resonance hazard of the *LCL*-filter [2], damping solutions are needed for the grid connected inverters to stabilize the system. In addition to the resonance hazard, the grid-connected inverter with an *LCL*-filter is more sensitive to the grid voltage. Therefore, the control scheme dominates the injected grid current harmonics caused by the grid voltage distortion, which is significant for the grid-connected inverter with an *LCL*-filter. IEEE Standard (1547- 2003) [3] gives the limitation of the injected grid current harmonics.

Mainly, there are two ways to suppress the injected grid current harmonics caused by the grid voltage distortion. One way is realizing infinite loop gain at the harmonic frequencies. In [4-6] the proportional-integral (PI) regulators together with multiple proportional-resonant (PR) regulators in the synchronous *dq* frame are implemented. With these control schemes, the steady-state error of the injected grid current is eliminated and the low order injected grid currents harmonics are effectively concealed. The other way is using feedforward scheme. The feedforward scheme will not affect the loop gain of the system, and the stability of the system will not be affected as a consequence. In [7-8], the proportional feedforward of the filter capacitor voltage was introduced to eliminate the steady-state error of the inverter-side inductor current. The full-feedforward scheme of the grid voltage for a single-phase grid-connected inverter with an *LCL*-filter was derived [9]. This full-feedforward function of the grid voltage consists of three parts, which were the proportional, derivative and second derivative parts. With this full-feedforward scheme, the injected grid current

harmonics caused by the grid voltage distortion were effectively reduced.

Passive and active damping solutions the *LCL*-filter have been comprehensively discussed in literature [2, 10 and 11]. An analytical design approach for passively damping *LCL*-filters was discussed in [10]. Moreover, the passively damped filter may downgrade to a second-order system, which will definitely compromise its attenuation factor at higher frequencies, and hence neutralizing those benefits originally introduced by the undamped filters. The underlying reason is related to the theoretical fact that at certain frequencies, the resulting network may appear to have zero or very low impedance, inferring resonances and hence closed-loop instability. A straightforward method to dampen this resonance is to add real passive damping resistors in series with the filter capacitors.

On the other hand, implementation of active damping requires more sensors for sensing the filter capacitor currents [2, 12 and 13], voltages [11], [14] or both if complete state feedback is preferred [15]. In [11] explored various active damping approaches for *LCL*-filters and compared their performances of resonance damping. Certainly, the overall system costs and realization complexity will increase, which is commonly unattractive. That then leads to the development of a number of sensorless active damping methods [16-23], where the required control variables were obtained either through estimation from dc-link voltage and switching duty ratios, or using complex state observers. Unfortunately, the performance of such methods may largely depend on the accuracy of plant parameters, which are usually unknown or vary over a wide range, especially for complex power systems.

Two current feedbacks for *LCL*-filter are used to increase the flexibility of the overall system. Measuring the grid current or converter current, or even their weighted value for the re-organized *LCCL* filter is studied in [24]. In [25-27], grid current feedback was preferred, after it was specifically shown through root locus analysis to be slightly more stable than converter current feedback.

In this paper comprehensively investigates the intrinsic damping characteristic of a *LCL*-filter. This inherent damping term can be used for optimal damping of the *LCL* resonance without demanding for additional passive or active damping, as long as the filter component values are designed properly. Although, inherent damping is not exist when the grid current is measured for feedback control. This is leading to a conclusion that converter current feedback is more stable than grid current feedback. A simple approach for tuning the damping factor is proposed, which would preserve the advantage of using only one set of current sensors, but at the expense of a more compromised transient response. The controller algorithm and the proposed damping tuning technique used are implemented by using Cooperative Bacteria Foraging Optimization (CBFO). Results for endorsing those findings are given and ultimately showing mutual agreement.

2 System Modeling

Fig. 1 shows the grid-connected three-phase PWM voltage source inverter diagram through an *LCL*-filter. The following assumptions are considered:

- All the equivalent series resistance for grid-side filter inductor, inverter-side filter inductor, filter capacitor and transformer inductor are neglected.
- The ac supply voltages contain only positive-sequence fundamental component.

By applying both assumptions, and by aids of Fig. 2, the plant model transfer function Gp(s) is deduced as:

$$L_{gt} = L_g + L_{tr} \tag{1}$$

$$V_{inv}(s) = (L_{inv}s + \frac{1}{C_f s})I_{inv}(s) - (\frac{1}{C_f s})I_g(s) \tag{2}$$

$$I_{inv}(s) = (L_g C_f s^2 + 1)I_g(s) \tag{3}$$

By substituting Eq.(2) in Eq.(1), the $G_p(s)$ can be expressed as:

$$G_p(s) = \frac{I_g(s)}{V_{inv}(s)} = \frac{1}{L_{inv}L_{gt}C_f s^3 + (L_{inv} + L_{gt})s} \tag{4}$$

$$\frac{I_c(s)}{I_g(s)} = L_{gt}C_f s^2 \tag{5}$$

where v_{inv}, i_{inv}, i_g, and i_c represent the inverter voltage, inverter current, grid current and filter capacitor current in the time domain, respectively, while their capitalized notations are for representing them in the *s*-domain. L_{inv}, L_g, and L_{tr} stand for inverter-side filter inductor, grid-side filter inductor and transformer inductor, respectively and Cf is the capcitor filter.

The PWM inverter can be modeled as a linear amplifier with a delay. The delay can combined with the current PI controller. The transfer-function of the PI current controllers in *dq* reference frame is:

$$G_c(s) = K_p V_{dc}(1 + \frac{1}{\tau_c s}) \tag{6}$$

where K_p, τ_c, and V_{dc} represent the proportional gain, integral time-constant of PI controller and dc-link voltage, respectively.

2.1 Grid-current Feedback

Fig. 3(a) illustrates the control block diagram of *LCL*-filter-based three-phase PWM inverter with grid current feedback. From Eqs, (4 and 6), the system open-loop transfer function is:

$$\frac{I_g(s)}{I_g^*(s)-I_g(s)} = G_C(s)G_p(s) = \frac{K_p V_{dc}(s+\frac{1}{\tau_c})}{L_{inv}L_{gt}C_f s^4 + (L_{inv}+L_{gt})s^2} \quad (7)$$

Eq.(7) shows the absent of third order term in the characteristic equation, implies that:

- The overall closed-loop system is challenging to be stable,
- Even if a passive element (*R*) is included, it is generally inadequate to assure a well-damped plant.
- The plant response is dynamically slow with a small control bandwidth.

Improvement of this technique can be done by adding either external passive or active damping to limit the infinite gain at the *LCL* response frequency [25].

2.2 Converter-current Feedback

The converter current can be sensed for feedback control as shown in Fig. 3(b). Since the grid current is not directly controlled, the *q*-axis current reference should be set to $\omega_o C_f v_g$ (v_g is the phase grid voltage) instead of zero, where ω_o is the fundamental angular frequency. This is to guarantee unity power factor operation. Fig.3 (b) is modified to Fig.3(c) to be more convenient in performing the open loop analysis. The converter current can be expressed as the summation of the grid current and filter capacitor current as shown in Fig. 3(c).

Contrasting Fig. 3(c) with Fig. 3(a) shows that converter current feedback is equivalent to grid current feedback, with an additional i_c term added to the forward path. The open loop transfer function from Fig, 3(c) can be expressed as follows:

$$\frac{I_g(s)}{I_g^*(s)-I_g(s)-I_c(s)} = G_c(s)G_p(s) = \frac{K_p V_{dc}(s+\frac{1}{\tau_c})}{L_{inv}L_{gt}C_f s^4 + (L_{inv}+L_{gt})s^2} \quad (8)$$

Substitute by Eq. (5) in Eq.(8):

$$\frac{I_g(s)}{I_g^*(s)-I_g(s)} = \frac{K_p V_{dc}(s+\frac{1}{\tau_c})}{L_{inv}L_{gt}C_f s^4 + K_p V_{dc}L_{gt}C_f s^3 + (\frac{K_p V_{dc}L_{gt}C_f}{\tau_c} + L_{inv}L_{gt})s^2} \quad (9)$$

Compare the denominators in Eq, (7) by Eq. (9), it is clear that the latter has an additional s^3-term, which would provide damping by shifting two of its poles further into the left half plane, while the remaining two poles remain at the origin. The damping initiated can be adjusted by tuning the controller gains and the passive parameters to the coefficient of s^3-term.

Eq. (9) can be rewritten as:

$$\frac{I_g(s)}{I_g^*(s)-I_g(s)} = \frac{K_p V_{dc}(s+\frac{1}{\tau_c})}{[L_{inv}L_{gt}C_f s^2 + K_p V_{dc}L_{gt}C_f s + (\frac{K_p V_{dc}L_{gt}C_f}{\tau_c} + L_{inv}L_{gt})]s^2} \quad (10)$$

For a second order characteristic equation in the brackets given in Eq. (10), tuning should be done until the following condition is met:

$$\frac{K_p V_{dc}}{L_{inv}} = 2\xi\omega_{res} = 2\xi\sqrt{\frac{\frac{K_p V_{dc}L_{gt}C_f}{\tau_c} + L_{inv} + L_{gt}}{L_{inv}L_{gt}C_f}} \quad (11)$$

where,

$$\omega_{res} = \text{undamped resonance frequency} = \sqrt{\frac{\frac{K_p V_{dc}L_{gt}C_f}{\tau_c} + L_{inv} + L_{gt}}{L_{inv}L_{gt}C_f}} \quad (12)$$

As the integral term of the PI controller typically does not affect the resonance frequency extensively, therefore $\frac{K_p V_{dc}L_{gt}C_f}{\tau_c} \approx 0$ and the ω_{res} expression can be simplified to:

$$\omega_{res} \approx \sqrt{\frac{L_{inv}+L_{gt}}{L_{inv}L_{gt}C_f}} \quad (13)$$

To assess an *LCL*-filter, two aspects should be considered [27]:

- The selected inductors and capacitor should be as small as possible if the *LCL*-filter can fulfill the design requirement.
- To achieve good filter effect at the switch frequency the harmonic attenuation rate *f* can be used to evaluate the harmonic components.

3 Optimum Damping Control of LCL-Filter

The Bode plots in Fig. 4 show the frequency response of the *LCL*-filter. From those plots, it is clear that the *LCL*-filter has approximately the same magnitude response as an *L*-filter over the low frequency range and under various damping factors. Their phase response is, however, quite different with the maximum phase lag of an *L*-filter being $\pi/2$ radius, while

that of an *LCL*-filter always exceeding this value. The amount in excess of the *LCL*-filter would grow larger as the damping factor and operating frequency increase. As a result of the differences in phase, two design recommendations are suggested:

- The damping factor of *LCL* resonance is optimally adjusted.
- The dependence of the system crossover frequency (ω_c) with reference to its damping factor (ζ) and resonance frequency (ω_{res}). Fig. 4 shows that ω_c is mainly limited by the phase lag of the *LCL*-filter, the better guideline is to select ω_c as a fraction of the undamped resonance frequency, therefore:

$$\alpha = \frac{\omega_c}{\omega_{res}} \tag{14}$$

The system phase margin (ϕ_{LCL}) can be estimated by taking the time delay T_d of the PWM inverter into consideration as follows:

$$\phi_{LCL} = \frac{\pi}{2} - \omega_c T_d - \arctan\left(\frac{2\xi\alpha}{1-\alpha^2}\right) \tag{15}$$

Upon determining ω_c, , the proportional gain of the PI controller and the system crossover frequency are simply related by [14]:

$$K_p \approx \frac{\omega_c (L_{inv} + L_g)}{V_{dc}} \tag{16}$$

Combining Eqs. (11), (14) and (16) gives the following relationship between L_{inv} and L_g, $2\xi L_{inv} = \alpha(L_{inv} + L_g)$

$$\frac{L_{inv}}{L_g} = \frac{\alpha}{2\xi - \alpha} \tag{17}$$

4 Design Tools

4.1 Cooperative Bacteria Foraging Optimization (CBFO)

To improve the performance of the original Bacterial Foraging Optimization (BFO) algorithm the Cooperative BFO (CBFO) is introduced [21], which has a significant improvement in terms of convergence speed, accuracy and robustness. It can be classified into CBFO-S and CBFO-H, in which, CBFO-S is the serial heterogeneous cooperation on the implicit space decomposition level and CBFO-H is the serial heterogeneous cooperation on the hybrid space decomposition level [26].

The CBFO-H Algorithm consists of two search stages working in a serial fashion. The first stage, which applied the original BFO model with a large run-length unit parameter C_L, runs for a number of iterations to locate promising regions that including the global optimum. Then the algorithm passes the best found solutions to the next stage. The second stage reinitializes the bacteria colony in these best-so-far positions with a smaller run-length unit parameter C_S. and applies the explicit space decomposition cooperative approach to the BFO. This approach relies on splitting the search space (n-dimensional vector) into n/2 subspaces (which is 2-dimensional vector), where each subspace is optimized by a separate bacteria colony. The overall solution is the vector combining the best bacterium of each colony. This algorithm works by sequentially passing over the colonies: to evolve all the bacteria in colony *j*, the other n/2-1 components in the overall solution are kept constant (with their values set to the global best bacteria from the other n/2-1 colonies); then the j^{th} colony evolves and replace the j^{th} component of the overall solution by its best bacterium [26].

TABLE 1. THE PSEUDOCODE OF CBFO-H [26]

The pseudocode of CBFO-H
Stage 1: the original BFO algorithm **INITIALIZE:** the position and the associated run-length unit C_L of the bacteria colony; ***For*** (each chemotactic step $t = 1 : N_c^{s1}$) ***For*** (each bacterium $i = 1 : S$) **TUMBLE**; **RUN**; **REPRODUCTION**; **ELIMINATION & DISPERSAL**; ***End for*** ***End for*** **PASS** the best found solutions of each bacterium to stage 2; **Stage 2:** the multi-colony cooperative BFO algorithm using explicit space decomposition **REINITIALIZE:** bacteria positions from the best found solutions and the associate run length unit C_S. **SPLIT** the whole population into n/2 separate colonies of 2D vectors; ***For*** (each chemotactic step $t = 1 : N_c^{s2}$) ***For*** (each colony $j = 1 : n/2$)

For (each bacterium $i = 1 : S$)
TUMBLE;
RUN;
REPRODUCTION;
ELIMINATION & DISPERSAL;
End for
UPDATE the best bacterium replace the j^{th} component of the overall solution;
End for
EVOLUTION: Evolution is added to run-length unit by:
If (t ***mod*** β= 0) // β is user-defined constant.
$C(t+1) = C(t)/\alpha$; // α is user-defined constant.
End if
End for

The pseudocode of CBFO-H is described in Table 1 where N_c^{s1} and N_c^{s2} represent the number of chemotactic steps in stage 1 and 2 respectively, and α>1 is a user-defined constant that is used to decrease the run-length unit C.

4.2 LCL-Filter Design Algorithm

The *LCL*-filter parameters are designed by using CBFO. The CBFO algorithm is employed based on optimal damping control of the *LCL*-filter. The step by step design algorithm is:

- The bacteria in colony of HBF-PSO algorithm can be denoted by a set of 4-dimentional vector:
  $N = [L_g \quad L_{inv} \quad C_f \quad \omega_{sw}]$.
- Select C_f : to avoid a low power factor. The reactive power that caused by the filter capacitor C_f should be less than 5% of the rated active power. Therefore,
  $$C_f < \left(\frac{5}{100} . \frac{P}{3.2\pi.50.E^2} \right) \quad (20)$$
  where, P is the rated active power of the system and E is the RMS value of the grid voltage.
- Select α and ς for optimal damping control of the *LCL*-filter. The recommended values for optimal control are ζ = 0.707 at α=0.3 [23]. When the damping factor ζ decreased to 0.5, a higher crossover frequency ω_c can be obtained as shown in Fig. 4 and hence it yield to faster current control loop response. Therefore α and ζ can selected from the following inequalities:
  $$0.2 \le \alpha \le 0.4$$
  $$0.4 \le \xi \le 0.9 \quad (21)$$
- Select L_g and L_{inv} by using Eq. (17) and $\frac{L_{inv}}{L_g} < 2.5$
- Fitness function (J): uses the harmonic attenuation rate given in Eq. (22). To achieve good filter effort, If not, go to step 3.
  $$f = Minimize\ J = \frac{i_g(h_{sw})}{i_{inv}(h_{sw})} = \frac{\frac{1}{C_f L_g}}{\left|\omega_{res}^2 - \omega_{sw}^2\right|} \quad (22)$$
- Calculate if the designed parameters can fulfill the requirement of the resonance frequency. If not, go to step 3. To avoid resonance at lower order or high order frequency, the resonance frequency should be :
  $$1000\pi < \omega_{res} < \omega_{sw} \quad (23)$$
  where, ω_{res} is given in Eq. (13).

5 Results

In order to confirm the effectiveness of the proposed system, a MATLAB/Simulink model has been implemented. The schematic diagram of grid-connected PWM voltage source inverter with the proposed control system is given in Fig. 5. The CBFO algorithm is used to determine the best set of parameters for the *LCL*- filter and the best proportional constant of the PI current controller. *LCL*-filter parameters are: L_{gt} =1.7mH, L_{inv} = 1.2mH, C_f = 27μF, ω_c =314 rad/sec and V_{dc} = 300V. The switching frequency is 5 KHz and the deadtime is 2μs. The CBFO algorithm takes 87 iterations to generate the designed parameters for the *LCL*-filter and the PI current controllers as shown in Fig. 6.

The α and ζ can be selected from the inequalities in Eq.(19). To test the optimal damping control capability and to show how it affect inverter and grid currents, the HBF-PSO algorithm was run at α=0.3 and three damping gain values ζ=0.4, 0.9 and 0.7 respectively. Fig. 7(a, c and e) show the grid voltage and current and the inverter current at α=0.3 and ζ=0.4, 0.9 and 0.7 respectively. Fig. 7(b, d, and f) show the harmonics contents of grid current for the three-grid currents in Fig. 7(a, c, and e). The total harmonic distortion for the grid current in

the three figures are: 9.35 %, 5.98% and 2.14% respectively. Consequently, the dynamic performances of the simulated system are presented in Fig. 8 and 9. The current reference is stepped up from 7A to 22A in Fig. 8, and stepped down from 22A to 7A in Fig. 9. Both figures, show that the grid current is well regulated under both steady-state and transient operations. There is no overshoot in the current response observed during the two dynamic responses. This confirms that, the good damping performance of the proposed control scheme is successfully engaged.

6 Conclusion

This paper is focused on designing a Cooperative Bacteria Foraging Optimization (CBFO) algorithm of optimal damping LCL filter for three-phase PWM grid inverter. The main objective is to provide the design procedure for the *LCL*-filter that allows the optimum damping attained with a desired system control bandwidth. Mathematical analysis has been presented to study the steady-state and dynamic performances of the overall system. The fascination of the proposed control techniques is that they only desire one set of current sensors for implementing the feedback control and momentarily performing the necessary damping of *LCL* resonance. The proposed system is simulated by using MATLAB. It is concluded that the CBFO are a good solution to find the best parameters for the *LCL*-filters and the proportional gain of the PI current controller. Results presented validate the theoretical inference developed in this paper.

References:

[1] E.H.E.Bayoumi, "Dual-Input DC-DC Converter for Renewable Energy," *Electromotion Scientific Journal*, vol. 21, no. 1-2, pp.77-84, Jan-June 2014.

[2] E. Twining and D. G. Holmes, "Grid current regulation of a three phase voltage source inverter with an LCL input filter," *IEEE Trans. Power Electron.* , vol. 18, no. 3, pp. 888–895, May 2003.

[3] E.H.E.Bayoumi, "A Simplified Method for Controlling DC-DC Converters Using Sliding Mode Control," *in Proc. of the IASTED International Conf., Modelling Simulation and Identification*, MIC'03, Innsbruck, Austria, Feb2003, pp1-6.

[4] M. Liserre, R. Teodorescu, and F. Blaabjerg, "Multiple harmonics control for three-phase grid converter systems with the use of PI-RES current controller in a rotating frame," *IEEE Trans. Power Electron*., vol. 21, no. 3, pp. 836–841, May 2006.

[5] M. Liserre, R. Teodorescu, and F. Blaabjerg, "Stability of photovoltaic and wind turbine grid-connected inverters for a large set of grid impedance values," *IEEE Trans. Power Electron*., vol. 21, no. 1, pp. 263–272, Jan. 2006.

[6] P. Xiao, K. A. Corzine, and G. K. Venayagamoorthy, "Multiple reference frame-based control of three-phase pwm boost rectifiers under unbalanced and distorted input conditions," *IEEE Trans. Power Electron*., vol. 23, no. 4, pp. 2006–2017, Jul. 2008.

[7] A.Maamoun, E.H.E.Bayoumi, M.O.Khalil, and A.Mhfouz, "Converter-Inverter System WITH Dependent PWM Control FOR Three-Phase Induction Motor," *in Proc. of International Symposium on Advanced Control of Industrial Processes*, SICE2002, Kumamoto, Japan, June 2002, pp.91-96.

[8] S. Y. Park, C. L. Chen, J. S. Lai, and S. R. Moon, "Admittance compensation in current loop control for a grid-tie LCL fuel cell inverter," *IEEE Trans. Power Electron*, vol. 23, no. 4, pp. 1716–1723, Jul. 2008.

[9] X. Wang, X. Ruan, S. Liu and C. K. Tse, "Full feedforward of grid voltage for grid-connected inverter with LCL filter to suppress current distortion due to grid voltage harmonics," *IEEE Trans. Power Electron.*, vol. 25, no. 12, pp. 3119–3127, Dec. 2010.

[10] M. Liserre, F. Blaabjerg, and S. Hansen, "Design and control of an LCL-filter-based three-phase active rectifier," *IEEE Trans. Ind. Appl.*, vol. 41, no. 5, pp. 1281–1291, Sep./Oct. 2005.

[11] J. Dannehl, F. W. Fuchs, S. Hansen, and P. B. Thøgersen, "Investigation of active damping approaches for PI-based current control of grid-connected pulse width modulation converters with LCL filters," *IEEE Trans. Ind. Appl.*, vol. 46, no. 4, pp. 1509–1517, Jul./Aug. 2010.

[12] F. Liu, Y. Zhou, S. X. Duan, J. J. Yin, B. Y. Liu, and F. R. Liu, "Parameter design of a two-current-loop controller used in a grid-connected inverter system with LCL-filter," *IEEE Trans.*

Ind. Electron., vol. 56, no. 11, pp. 4483-4491, Nov. 2009.

[13] Y. Chen and F. Liu, "Design and control for three-phase grid-connected photovoltaic inverter with LCL-filter," in *Proc. 2009 IEEE Circuits and Systems International Conf.*, pp. 1-4.

[14] V. Blasko and V. Kaura, "A novel control to actively damp resonance in input LC filter of a three-phase voltage source converter," *IEEE Trans. Ind. Appl.*, vol. 33, no. 2, pp. 542-550, Mar./Apr. 1997.

[15] E. Wu and P. W. Lehn, "Digital current control of a voltage source converter with active damping of LCL resonance," *IEEE Trans. Power Electron.*, vol. 21, no. 5, pp. 1364-1373, May 2006.

[16] J. Dannehl, F. W. Fuchs, S. Hansen, and P. B. Thogersen, "Investigation of active damping approaches for PI-based current control of grid-connected pulse width modulation converters with LCL-filters," *IEEE Trans Ind. Appl.*, vol. 46, no. 4, pp. 1509-1517, Jul./Aug. 2010.

[17] H.G. Jeong, K. B. Lee, S. Choi, and W. Choi, "Performance improvement of LCL-filter-based grid-connected inverters using PQR power transformation," *IEEE Trans. Power Electron.*, vol. 25, no. 5, pp. 1320-1330, May 2010.

[18] S. Mariethoz and M. Morari, "Explicit model-predictive control of a PWM inverter with an LCL-filter," *IEEE Trans. Ind. Electron.*, vol. 56, no. 2, pp. 389-399, Feb. 2009.

[19] L. A. Serpa, S. Ponnaluri, P. M. Barbosa and J. W. Kolar, "A modified direct power control strategy allowing the connection of three-phase inverters to the grid through LCL-filters," *IEEE Trans. Ind. Appl.*, vol. 43, no. 5, pp. 1388-1400, Sep./Oct. 2007.

[20] Ehab H.E. Bayoumi," Design and Control of an LCL Series Parallel Resonant Converters Using Bacterial Foraging Optimization," *International Journal of Power Electronics (IJPELEC)*, Vol.4, No.5, pp. 497-504, 2012.

[21] E.H.E. Bayoumi, "Parameter Estimation of Cage Induction Motors Using Cooperative Bacteria Foraging Optimization," *Electromotion Scientific Journal*,Vol.17, No.4, pp.247-260, Oct.-Dec.2010.

[22] Ehab H.E. Bayoumi, "Minimal Overshoot Direct Torque Control for Permanent Magnet Synchronous Motors Using Hybrid Bacteria Foraging-Particle Swarm Optimization," IEEE Symposium Series on Computational Intelligence (SSCI 2013), IEEE Symposium on Computational Intelligence in Control and Automation, 15-19 April, Singapore, 2013, pp. 112-119.

[23] E.H.E.Bayoumi, A.Maamoun, O.Pyrhönen, M.O.Khalil, and A.Mhfouz, "Enhanced Method for Controlling PWM Converter-Inverter System," *in Proc.of the IASTED International Conf. of POWER AND ENERGY SYSTEMS*, PES'02, California, USA, May2002, pp. 425-430.

[24] G. Shen, D. Xu, L. Cao, and X. Zhu, "An improved control strategy for grid-connected voltage source inverters with an LCL-filter," *IEEE Trans. Power Electron.*, vol. 23, no. 4, pp. 1899-1906, Jul. 2008.

[25] J. Dannehl, C. Wessels, and F. W. Fuchs, "Limitations of voltage-oriented PI current control of grid-connected PWM rectifiers with LCL-filters," *IEEE Ind. Electron.*, vol. 56, no. 2, pp. 380-388, Feb. 2009.

[26] Ehab H.E. Bayoumi, "Matrix Converter for Static Synchronous Series Compensator using Cooperative Bacteria Foraging Optimisation", *Intentional Journal of Industrial Electronics and Drives (IJIED)*, Vol.1, No. 2, pp. 73-81, 2014.

[27] R. Teodorescu, F. Blaabjerg, M. Liserre, and A. Dell'Aquila, "A stable three-phase LCL-filter based active rectifier without damping," in *Proc. 2003 IEEE Industry Applications Society Annual Meeting*, pp. 1552-1557.

[28] Y. Tang, P. C. Loh, P. Wang, F. H. Choo, and K. K. Tan, "Improved one cycle- control scheme for three-phase active rectifiers with input inductor capacitor- inductor filters," *IET Power Electron*, vol. 4, no. 5, pp. 603–614, 2011.

[29] E.H.E. Bayoumi and F.Salem, "PID controller for series-parallel resonant converters using bacterial foraging optimization," *Electromotion Journal*, vol. 19, no. 1-2, pp. 64-79, 2012.

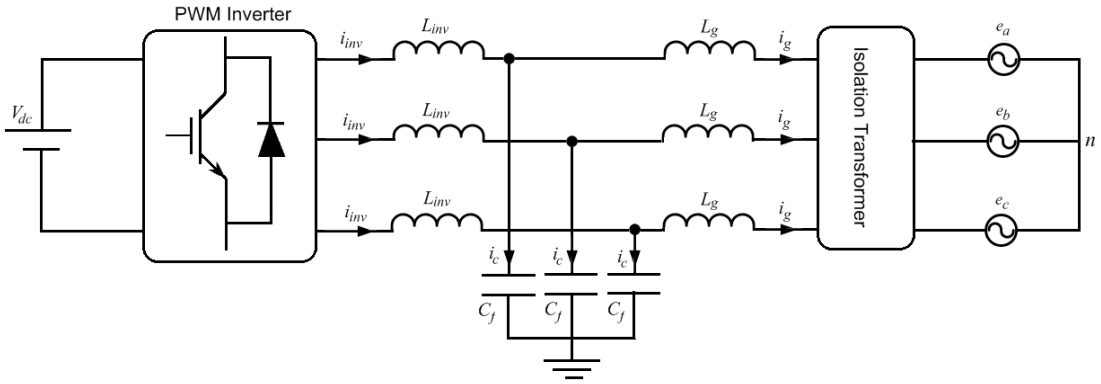

Fig. 1: The LCL-filter-grid-connected PWM inverter.

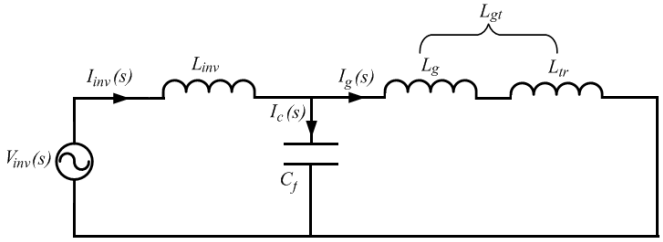

Fig.2: Equivalent circuit for LCL-filter- grid-connected PWM inverter.

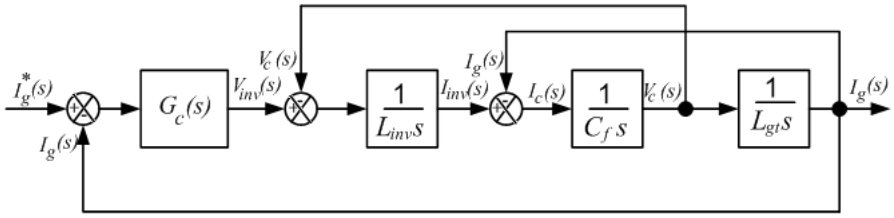

(a)

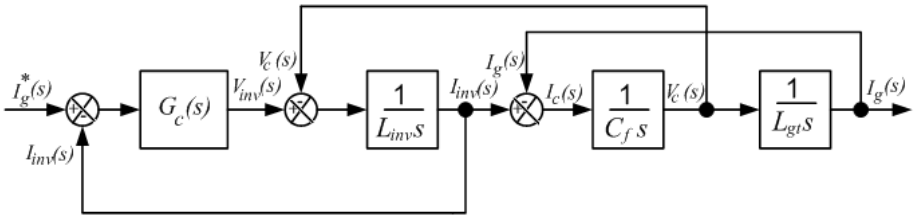

(b)

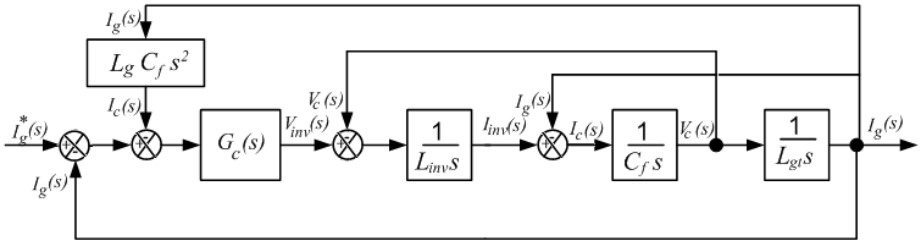

(c)

Fig. 3. Block diagram of (a) grid-current feedback control, (b) converter-current feedback control, and (c) equivalent converter-current feedback control.

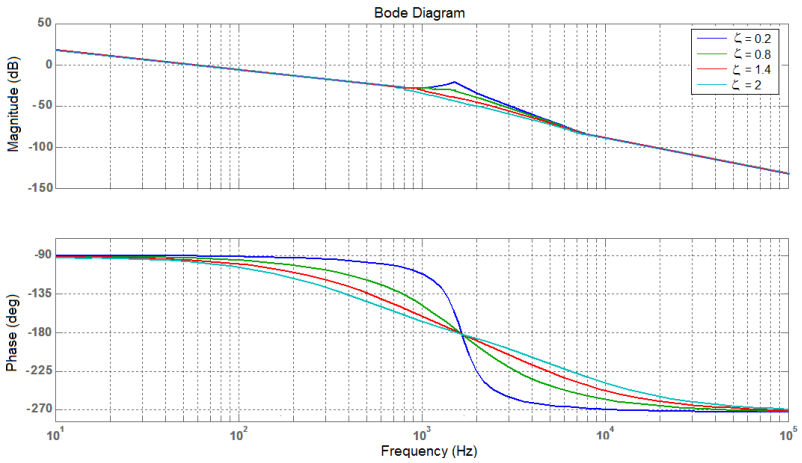

Fig. 4. Bode plots of LCL filter for several damping factors.

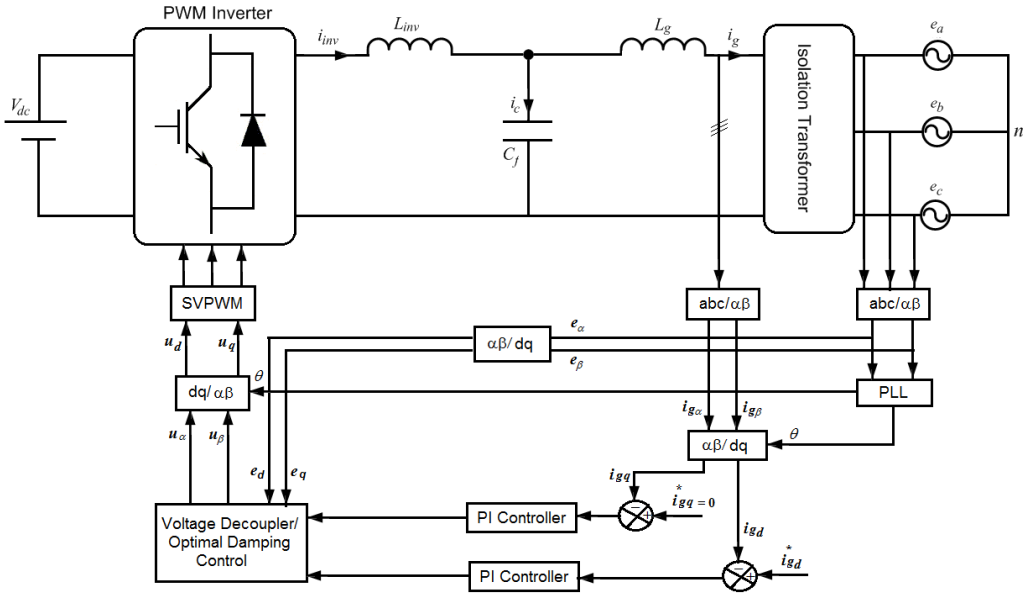

Fig.5. Schematic diagram of the proposed control technique.

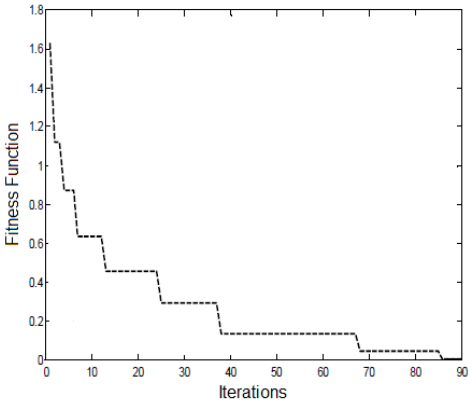

Fig. 6. Fitness function vs iterations.

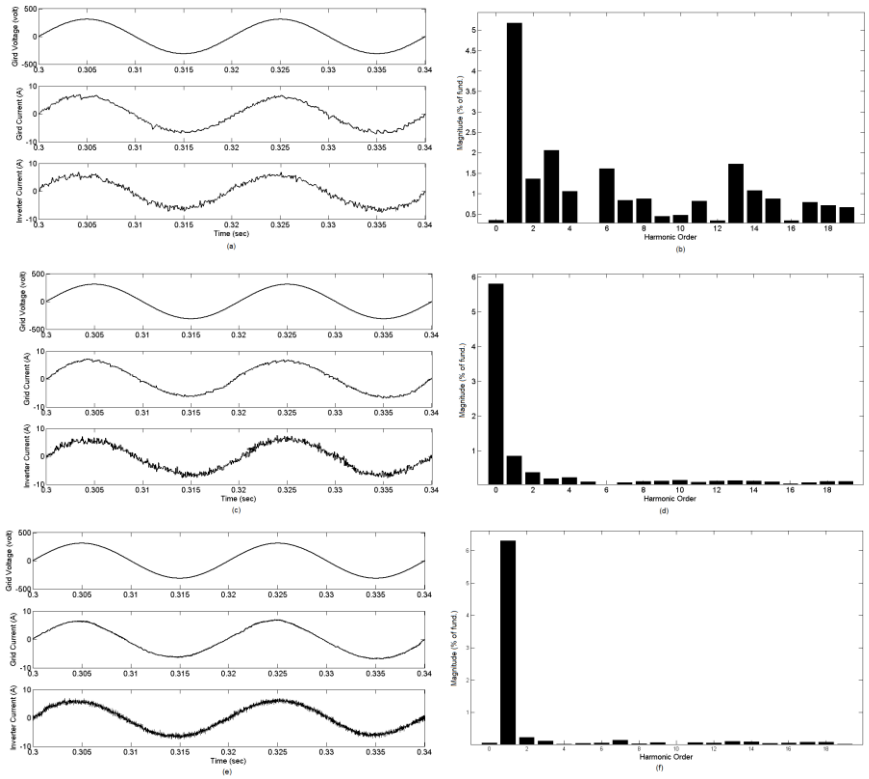

Fig. 7. (a, c, and e) Grid voltage and current and inverter current at ζ=0.4, 0.9, and 0.7 respectively, (b, d and f) harmonic contents of grid current at ζ=0.4, 0.9, and 0.7 respectively.

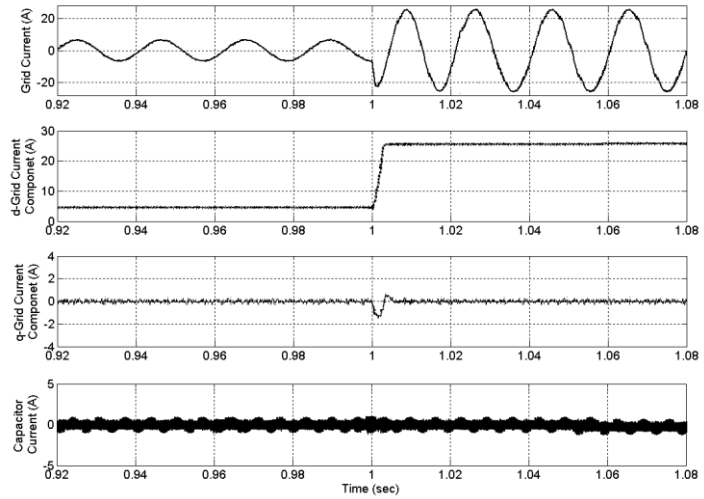

Fig.8. The *LCL*- filter-PWM inverter subjected to a step-up current reference from 7A to 22A.

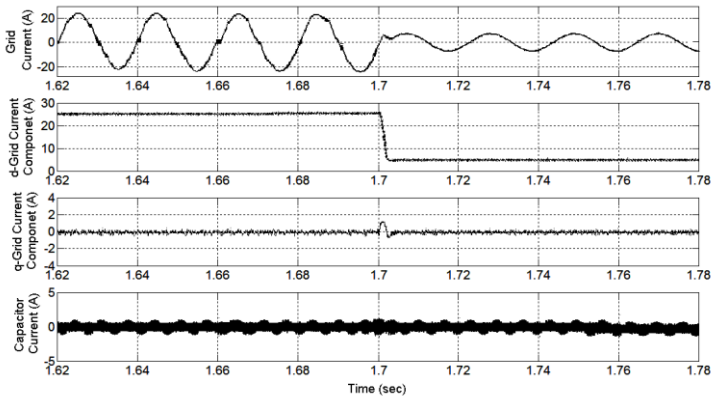

Fig. 9. The *LCL*- filter-PWM inverter subjected to a step-down current reference from 22A to 7A.